Available online at www.sciencedirect.com
ScienceDirect
Journal of the European Ceramic Society 30 (2010) 2481–2490
www.elsevier.com/locate/jeurceramsoc

Effects of SiO_2 addition on TiO_2 crystal structure and photocatalytic activity

David Maria Tobaldi [a,*], Antonella Tucci [a], Andrijana Sever Škapin [b], Leonardo Esposito [a]

[a] *Centro Ceramico Bologna, Via Martelli 26, 40138 Bologna, Italy*
[b] *Slovenian National Building and Civil Engineering Institute, Dimičeva 12, SI-1000 Ljubljana, Slovenia*

Received 24 August 2009; received in revised form 5 May 2010; accepted 18 May 2010
Available online 11 June 2010

Abstract

A series of TiO_2–SiO_2 mixtures – having the following stoichiometry $Ti_{1-x}Si_xO_2$, with $x = 0, 0.1, 0.3$ and 0.5 atoms per formula unit – were prepared by using precursor oxides and fired at three temperatures (900, 1000 and 1200 °C). The modifications in the structure and, consequently, on the photocatalytic activity, induced by the addition of SiO_2 into the TiO_2 powder, were thoroughly investigated by using various analytical techniques: X-ray powder diffraction, electron microscopy (FE-SEM and TEM), XPS, FT-IR, DRS and BET analysis. The results underlined as essentially no solid solution occurs between the two crystalline end-members. Nevertheless, silica addition caused a retarding effect on anatase-to-rutile phase transformation and on the crystallite growth.

The photocatalytic activity of the powders was assessed in gas phase and the results were explained by taking into account the anatase and rutile relative amounts in the samples, their crystallite size, the surface hydroxyl groups adsorbed on the photocatalysts and the surface area of the mixtures.

Keywords: TiO_2; X-ray methods; Photocatalysis; Traditional ceramics; Functional applications

1. Introduction

There are four naturally occurring polymorphs of TiO_2 – rutile (tetragonal, space group $P4_2/mnm$), anatase (tetragonal, space group $I4_1/amd$), brookite (orthorhombic, space group $Pbca$), and TiO_2 (B) (monoclinic, space group $C2/m$)[1] – the most thermodynamically stable of which is rutile. Both brookite and anatase transform into rutile upon heating exothermally and irreversibly, in a certain range of temperatures. Such a transformation is a metastable-to-stable irreversible transformation and it is widely accepted that the phase transition from brookite into rutile takes place in a temperature range of 500–600 °C,[2] whereas anatase transforms into rutile within a temperature range of 600–1100 °C.[3]

Anatase and rutile are TiO_2 polymorphic forms which are relevant in photocatalytic applications,[4] even if, for many authors, anatase is more photocatalytically active than rutile.[5–9] Moreover, being titanium dioxide compatible with the processing of silicate body mixes, the possibility to obtain photocatalytically active building materials could represent an alternative way to face the rising environmental pollution.

Anatase lattice is constituted by distorted TiO_6 octahedral sites, sharing four common edges[10]; while rutile one is composed of distorted TiO_6 octahedra where each octahedron shares two of its opposite edges with two other octahedra in order to form octahedral chains, running parallel to the c-axis.[11]

The anatase-to-rutile ($A \rightarrow R$) polymorphic phase transformation follows a nucleation-growth mechanism.[12] Upon thermal treatment, anatase crystallites grow until they reach a critical nuclei size; once overcome, the rutile nucleation starts,[13] involving the breaking of the anatase Ti–O bonds, followed by a cooperative motion of these atoms.[14] The $A \rightarrow R$ phase transformation is influenced by several factors, such as grain size,[15] crystallite dimension,[16] atmosphere[17] and the presence of dopants.[18]

Anatase is a well known and studied photocatalyst,[19] but its polymorphic transformation to rutile is considered to be a drawback that limits the photocatalytic activity. Differently, high specific surface area[20] as well as crystallinity[21] positively affect the photocatalytic behaviour. Because the firing of TiO_2 leads to a decrease in surface area and an increase in crystallinity, it can be stated that, to a certain degree, a compromise between

* Corresponding author. Tel.: +39 051 534015; fax: +39 051 530085.
E-mail address: tobaldi@cencerbo.it (D.M. Tobaldi).

0955-2219/$ – see front matter © 2010 Elsevier Ltd. All rights reserved.
doi:10.1016/j.jeurceramsoc.2010.05.014

the crucial factors – temperature, A → R phase transformation, specific surface area and crystallinity – needs to be reached.

In literature, several metal oxides, such as Al_2O_3, ZrO_2 and SiO_2,[22–25] are added to titania in order to improve its UV photocatalytic activity, even if this property has not been tested for firings at high temperature. The addition of silica to TiO_2 could result rather attractive, not only because of its ability to maintain a charge balance, but also because silica is a low-cost, non-toxic and easily available product.

Actually, the system TiO_2–SiO_2 exhibits no miscibility at 10^5 Pa – despite Ti and Si are both tetravalent cations coordinated by oxygen – due to the significant differences between Ti^{4+} and Si^{4+} ionic radii; at pressure as high as 3 GPa, the solubility of SiO_2 in the TiO_2-rich liquid is slightly enhanced.[26] In fact, keeping to the present knowledge on the formation of TiO_2–SiO_2 solid solutions – TiO_2–SiO_2 phase diagram[27] – at the eutectic temperature (1550 ± 4 °C) cristobalite and rutile coexist in equilibrium with a liquid having such a composition: 10.5 wt% TiO_2 and 89.5 wt% SiO_2. According to those authors,[27] below the eutectic temperature, there is no solid solution between cristobalite and rutile, but these two coexisting solids.

The aim of the present work is to study the photocatalytic activity of a titania powder in which was added silica and which has been fired at high temperature for a likely employ on silicate based ceramic products.[28] The results are explained with regard to the impact that the crystallographic characteristics – determined coupling X-ray powder diffraction structural data with quantitative phase analysis ones – such as anatase and rutile relative amount in the mixture, their crystallite dimension and surface properties, exert on the photocatalytic activity of the investigated samples.

2. Experimental procedures

2.1. Sample preparation and characterisation

The TiO_2–SiO_2 mixes were prepared using two commercial powders as starting materials, a titania, Aeroxide P25 (DE), and a silica powder, CAB-O-SIL® EH-5 (US); their main characteristics are given in Table 1. The studied mixtures were prepared according to the following stoichiometry: $Ti_{1-x}Si_xO_2$ where $x = 0$, 0.1, 0.3 and 0.5 apfu.

The starting powders were thoroughly mixed in water (75 wt%) by using a high shear mixer (Silverson L4R, US), for 1 min. Then they were dried in oven at 110 °C and fired in a laboratory muffled furnace, subject to different thermal cycles in order to simulate the firing steps of silicate based products. Three maximum temperatures were reached – 900, 1000 and 1200 °C. Unmodified TiO_2, used as reference sample, was thermally treated at the same temperatures.

For the firing at 900 and 1000 °C, an heating rate of 7 °C/min, 4 h of soaking time at the maximum temperature and natural cooling was adopted as thermal cycle, with the aim of simulating the industrial firing of heavy-clay products. For the firing at 1200 °C, the same thermal cycle was used, the only difference was in the soaking time of 1 min, in order to simulate the firing steps adopted in the ceramic tiles production.

Samples in which silica was added, were named after the Si symbol, followed by the apfu amount added, and the value of the maximum temperature reached. Pure titania at room temperature was named after P25 symbol; when fired, the denomination with P25 was followed by the value of the maximum temperature reached.

In order to find out the phase composition, the unit cell parameters, Ti–O bond distances and the mean crystallite size, the powders were characterised through X-ray powder diffraction analysis, XRPD, by using a Panalytical X'Pert Pro diffractometer (NL) equipped with a fast RTMS detector,[29] with graphite monochromated Cu $K\alpha_{1,2}$ radiation (5–120° 2θ range, a virtual step scan of 0.0167° 2θ and 30 s per step). The powders crystal structure was refined using the Rietveld method and the refinements were carried out using GSAS-EXPGUI software packages.[30,31] The starting atomic parameters of anatase and rutile were taken from Howard et al.,[32] adopting $I4_1/amd$ space group for the former and $P4_2/mnm$ one for the latter. Depending upon the number of phases in the samples, up to 28 variables were refined: scale-factors, zero-point, 6 coefficients of the shifted Chebyshev function adopted to fit the background, unit cell parameters – determined using silicon (NIST SRM 640c) as internal standard – atomic positions, isotropic displacement parameters (U_{ISO}) and profile coefficients – one Gaussian, G_W, two Lorentzian terms, L_X and L_Y – peak correction for asymmetry and sample displacement effects. Quantitative phase analysis (QPA), via XRPD, was used to determine the amorphous amount by adding 10 wt% corundum (NIST SRM 676a) used as internal standard.[33] For this purpose the XRPD data collection extremes were: 10–80° 2θ range, 0.02° step scan and 5 s per step.

The distortion of the octahedral site, TiO_6, was estimated as bond length distortion (BLD):

$$\mathrm{BLD} = 10 \times \frac{\sum_i |(M\text{–}O)_i - \langle M\text{–}O\rangle|}{\langle M\text{–}O\rangle} \quad (1)$$

where $(M–O)_i$ is the ith metal–ligand distance and $\langle M–O\rangle$ is the average metal–ligand distance.[34]

Anatase and rutile mean crystallite size was calculated by measuring the broadening of the X-ray reflections from selected FWHM values: (1 0 1) crystallographic plane for anatase and (1 1 0) for rutile, using the Scherrer's formula (2), with Warren's correction (3) for instrumental broadening[35]:

$$t = \frac{k\lambda}{\beta \cos\theta} \quad (2)$$

Table 1
Phase composition and surface area of the starting powders.

Sample	Phase composition		S_{BET} ($m^2\ g^{-1}$)
	Anatase (wt%)	Rutile (wt%)	
AeroxideTiO_2 P25	85.6(1)	14.4(2)	50.0
CAB-O-SIL® EH-5	Amorphous silica		380.0

Note: values in parentheses are the standard deviations referred to the last decimal figure.

where t is the linear dimension of particle, k is the Scherrer's constant (0.9), λ is the wave-length of the incident X-rays, θ is the Bragg's angle and β is the sample line broadening (FWHM) that was calculated using LaB_6 (NIST SRM 660a) as line broadening standard:

$$\beta^2 = \beta_M^2 - \beta_S^2 \quad (3)$$

where β_M is the measured FWHM, β_S the instrumental contribution on the total FWHM.

The morphology of the powders was investigated by FE-SEM (Zeiss Supra 35-VP, DE) and by TEM (JEOL JEM, 2010, JP) equipped with an energy dispersion X-ray attachment, EDS (Inca, Oxford Instruments, GB). The atomic surface composition of the powders was evaluated through XPS analysis, carried out on a TFA XPS spectrometer (Physical Electronics, US); the spectra were recorded using monochromated Al Kα (1486.8 eV).

In order to find out the possible occurrence of OH groups adsorbed on photocatalysts surface and of Ti–O–Si bonds, FT-IR analysis was performed using a Perkin Elmer Spectrum One (US) and the scanning was set in the wavenumber range of 4000–400 cm^{-1}. The powders were mixed with KBr (2/200 by weight) and pressed into thin pellets.

Diffuse reflectance spectroscopy (DRS) was used with the aim to detect whether silica addition shifted or not titania absorption edge. Spectra were acquired in the UV–vis range (300–750 nm, 0.03 nm step size, $BaSO_4$ as reference) on a Perkin Elmer λ35 (US) spectrophotometer.

Their surface area was determined using the BET (Brunauer Emmett Teller) method (Flowsorb II 2300 Micromeritics, US) with N_2 as adsorbate gas.

2.2. Photocatalytic experiments

Photocatalytic activity of the powders was evaluated by monitoring the degradation of model organic compounds in gas medium by FT-IR. The tests were carried out by way of monitoring the oxidation of isopropanol into acetone and its subsequent degradation, using FT-IR spectroscopy, in a cylindrical reactor (1.4 L in volume) covered by a quartz glass. The light source was a 300 W Xenon lamp (Newport Oriel Instrument, US) having light intensity of ∼30 W/m^2 in the λ range of 315–380 nm. The infrared part of the spectrum was blocked by means of an adequate filter. The samples were prepared in the shape of thin layer of powder with constant thickness in a petri dish with 6 cm in diameter. The working distance between the petri dish and the lamp was 6 cm. Due to a strong influence of relative humidity on photocatalytic activity, the relative humidity at 23 °C in the system prior to the experiment was kept within the range of 25–30%. It was maintained such by means of a flow of synthetic air passing through the system. Relative humidity and temperature were controlled by thermo- and hygro-meter which was placed into the reactor. Each experiment was performed by injecting 3 μL of isopropanol (∼700 ppm in gas phase) into the reacting system through a septum. The total reaction time was set at 540 min and the lamp was turned on 60 min after the isopropanol injection, in order to complete the adsorption of isopropanol onto the powder. The isopropanol degradation and acetone formation–degradation processes were followed by monitoring the calculated area of their characteristic peaks at 951 and 1207 cm^{-1}, respectively, in the IR region measured by a FT-IR spectrometer (Perkin Elmer Spectrum BX, US) and analysed by software. We evaluated the photocatalytic activity as the rate of the initial acetone formation (during the first 10 min), because the slope is linear and thus acceptable for an evaluation only for short periods of time.[36] In addition, with acetone as the first intermediate of isopropanol degradation,[37] it may be considered that its formation is characteristic and distinguishing of isopropanol photo-oxidation.

3. Results and discussion

3.1. Titania structural modifications

As summarized in Tables 2–5, silica addition affected titania phase composition, mean crystallite size, surface area, and A → R phase transition temperature of the fired samples.

Whereas pure titania, sample P25, is completely transformed into rutile already at 900 °C, the addition of silica delayed the A → R polymorphic transformation (see Table 2). When fired at 900 °C, sample Si0.1, still contains 10.7 wt% of anatase, but also 8.0 wt% of amorphous phase; when fired at 1000 °C the anatase and amorphous amounts are 3.9 and 8.0 wt%, respectively. The A → R phase transformation is complete at 1200 °C, even if 7.9 wt% of amorphous phase still exists. The presence of 0.3 apfu of silica allows keeping the maximum anatase amount among the samples fired at 900 and 1000 °C, namely 49.4 and 31.2 wt%, respectively. When fired at 1200 °C, it still contains a small amount of anatase, 1.1 wt% as well. Si0.5 900 contains 42.7 wt% of anatase and 39.1 wt% of amorphous phase. By increasing the temperature, Si0.5 1000, the anatase and amorphous amounts are of 28.6 and 43.0 wt%, respectively. Si0.5 1200 contains the maximum anatase amount (2.0 wt%), and the

Table 2
Phase composition of pure titania and of the samples fired at the different temperatures.

Sample	Phase composition		
	Anatase (wt%)	Rutile (wt%)	Amorphous (wt%)
P25	85.6(1)	14.4(2)	0
P25 900	0	100	0
Si0.1 900	10.7(2)	81.3(1)	8.0(5)
Si0.3 900	49.4(1)	30.3(1)	20.3(4)
Si0.5 900	42.7(1)	18.2(1)	39.1(4)
P25 1000	0	100	0
Si0.1 1000	3.9(1)	88.1(1)	8.0(4)
Si0.3 1000	31.2(1)	45.4(1)	23.4(4)
Si0.5 1000	28.6(1)	28.4(1)	43.0(4)
P25 1200	0	100	0
Si0.1 1200	0	92.1(1)	7.9(3)
Si0.3 1200	1.1(1)	77.8(1)	21.2(4)
Si0.5 1200	2.0(1)	53.7(1)	44.3(4)

Note: values in parentheses are the standard deviations referred to the last decimal figure.

Table 3
Rietveld refinement parameters and unit cell parameters of pure titania and of the samples fired at the different temperatures.

Sample	Unit cell parameters						Rutile isotropic displacement parameters and oxygen position			Rietveld refinement parameters			
	Anatase			Rutile									
	$a=b$ (Å)	c (Å)	Volume (Å^3)	$a=b$ (Å)	c (Å)	Volume (Å^3)	U_{ISO} (Ti)	U_{ISO} (O)	x (O)	Variables	$R(F^2)$	R_{wp}	χ^2
P25	3.7857(2)	9.5078(8)	136.26(1)	4.5911(7)	2.9624(9)	62.44(2)	0.004	0.005	0.3186(27)	20	0.12	0.13	1.5
P25 900	–	–	–	4.5940(1)	2.9593(1)	62.46(1)	0.004	0.005	0.3049(1)	17	0.06	0.08	2.0
Si0.1 900	3.7862(1)	9.5082(5)	136.31(1)	4.5941(1)	2.9593(1)	62.46(1)	0.007	0.005	0.3052(3)	22	0.08	0.06	1.5
Si0.3 900	3.7860(1)	9.5076(3)	136.28(1)	4.5941(1)	2.9595(1)	62.46(1)	0.006	0.006	0.3053(5)	24	0.04	0.06	1.1
Si0.5 900	3.7855(1)	9.5069(3)	136.23(1)	4.5935(1)	2.9595(1)	62.45(1)	0.007	0.004	0.3061(6)	28	0.06	0.06	1.1
P25 1000	–	–	–	4.5937(1)	2.9593(1)	62.45(1)	0.006	0.005	0.3049(3)	20	0.08	0.10	1.9
Si0.1 1000	3.7864(9)	9.4955(48)	136.14(1)	4.5938(1)	2.9594(1)	62.45(1)	0.004	0.005	0.3058(4)	24	0.12	0.11	1.1
Si0.3 1000	3.7860(1)	9.5073(5)	136.28(1)	4.5942(1)	2.9594(1)	62.46(1)	0.005	0.005	0.3045(6)	25	0.06	0.09	1.0
Si0.5 1000	3.7856(1)	9.5069(3)	136.24(1)	4.5935(1)	2.9595(1)	62.45(1)	0.008	0.005	0.3063(6)	27	0.06	0.06	1.1
P25 1200	–	–	–	4.5936(3)	2.9591(2)	62.44(1)	0.004	0.006	0.3052(4)	18	0.15	0.14	1.4
Si0.1 1200	–	–	–	4.5928(2)	2.9605(1)	62.45(1)	0.004	0.006	0.3060(3)	18	0.09	0.10	1.2
Si0.3 1200	3.7829(12)	9.5130(50)	136.14(9)	4.5944(1)	2.9610(1)	62.50(1)	0.004	0.006	0.3052(4)	21	0.09	0.10	1.1
Si0.5 1200	3.7845(6)	9.5170(27)	136.31(5)	4.5958(1)	2.9616(1)	62.55(1)	0.005	0.004	0.3059(3)	23	0.09	0.08	1.4

Note: values in parentheses are the standard deviations referred to the last decimal figure.

maximum amorphous amount (44.3 wt%) in comparison with other samples fired at the same temperature. From the QPA results, the amorphous amount is approximately equal to the silica added to the titania powder in the starting formulation; additionally, we did not find any cristobalite nor the presence of any crystalline SiO_2, but amorphous phase as an evidence of silica immiscibility; it can be deduced that no silica – or at least a really small amount – should be found in the fired samples where silica was added in.

The unit cell parameters of the samples fired at the different temperatures, as well as the Rietveld refinement parameters, are reported in Table 3; an example of Rietveld refinement plot is depicted in Fig. 1, as an evidence of the accuracy of the results. From the structural data, the previous assumption, namely the silica immiscibility, is confirmed, indeed, by an analysis of rutile unit cell parameters: at 900 and 1000 °C, *a*- and *c*-axes of rutile contained in samples in which was added silica, show no change if compared to the ones of the reference sample (Table 3). From this finding, it can be inferred that no solid solution occurs between rutile and SiO_2.[38] Actually, according to the TiO_2–SiO_2 phase diagram,[27] such system shows no miscibility due to the significant differences between $^{[4,6]}Ti^{4+}$ and $^{[4,6]}Si^{4+}$ ionic radii (0.42–0.605 and 0.26–0.400 Å, respectively).[39] A small deviation from this trend is given by samples fired at the maximum temperature: the more the silica addition, the bigger the unit cell volume. Further studies are in progress, in order to clarify this trend.

The same assumption is made, considering anatase unit cell parameters: no solid solution takes place between silica and anatase.

The addition of silica to titania – as expected – slightly modified rutile Ti–O distances and hence the octahedral site rutile is coordinated (Table 4). Focusing on the BLD of fired samples, it can be assumed that silica addition vaguely promotes a distortion of the octahedral site, a part from samples Si0.3 fired at 1000 and 1200 °C that are somewhat less distorted than the reference one. Though Ti–O distances are compatible with absence of solid solutions, BLD trend is not in full agreement with the above-discussed immiscibility between the two oxides.

The analysis of the mean crystallite sizes of anatase and rutile in the prepared samples (see Table 5), indicates that silica addition limits not only the A → R phase transformation, but also the dimensional increase in all the samples (Fig. 2). While the mean crystallite size of P25 fired at 900 °C, 100% of rutile, is 103 nm (Fig. 2a), in the samples with silica addition, rutile crystallite size is always smaller and it continuously decreases with the amount of SiO_2 added. At 1000 °C, anatase crystallite size is in the range of 28–38 nm, following the same trend as the rutile particles (Fig. 2c and d). When fired at 1200 °C, rutile reached the maximum crystallite size, ranging from 66 to 126 nm.

As assessed by TEM observations of the samples in which silica was added (Fig. 3), larger titania particles are partially surrounded by finer silica ones. This way, the amorphous SiO_2 matrix behaves as a barrier, reducing the coarsening of anatase[40,41] by preventing titania particles from coming into mutual contact and therefore delaying the critical size beyond that anatase transforms to rutile.[42]

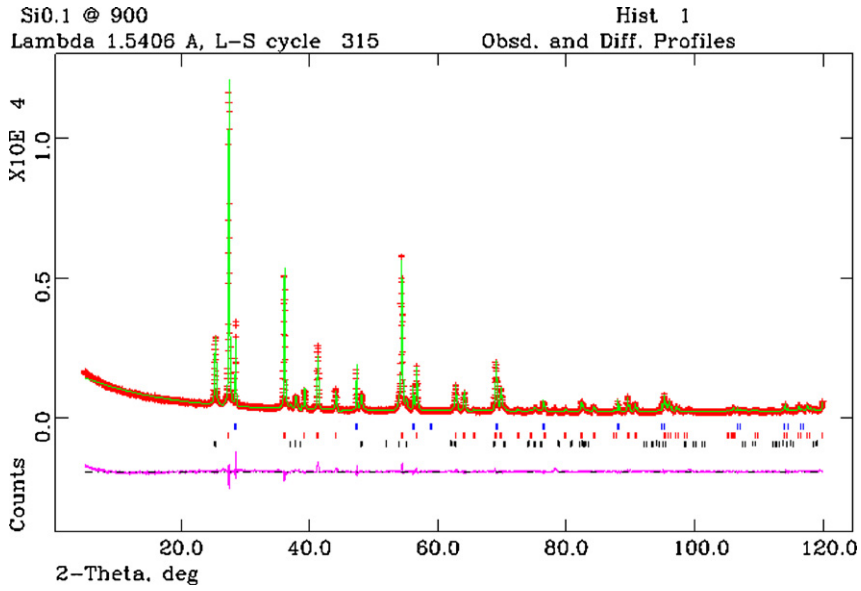

Fig. 1. Rietveld refinement plot of the X-ray powder diffraction data of the sample Si0.1 fired at 900 °C. The continuous green line represents the calculated pattern, while the red cross points stand for the observed pattern; the difference curve between observed and calculated profiles is plotted below. The position of reflections is indicated by the small vertical bars (black: anatase; red: rutile; blue: silicon, the internal standard). (For interpretation of the references to color in this figure legend, the reader is referred to the web version of the article.)

The surface area of the samples in which silica was added, when fired at the same temperature, increases proportionally with the SiO_2 amount added, due to the larger amount of nano-sized silica that is around titania particles. In addition, the increase of the thermal treatment temperature, from 900 to 1200 °C, induces a drastic decrease of the surface area for the whole set of samples, due to incipient sintering effects among the different particles (Table 5).

3.2. FT-IR, DRS and XPS characterisation

FT-IR spectra (Fig. 4), show different absorption bands in the range of 400–600 cm^{-1} to be attributed to Ti–O–Ti vibrations,[43] while the peak at ~1620 cm^{-1} corresponds to the bending vibrations of O–H, and the broad bands at around 2840 and 3430 cm^{-1} are attributed to the surface adsorbed water and hydroxyl groups.[44] These two latter bands are stronger in the fired samples in which was added silica (Fig. 4c) than in the pure and fired one (Fig. 4b), suggesting that the addition of silica brings more surface hydroxyl groups to the photocatalysts. The faint band at about 960 cm^{-1} observed in sample Si0.1 (Figs. 4c and 5) has been attributed to the asymmetric stretching vibration of Ti–O–Si bond[45]: TiO_2 and SiO_2 are probably not only as single oxide but they also form complex oxide particles.[46] Moreover, in the samples in which was added silica, there is a peak at approximately 1070 cm^{-1} which can be

Table 4
Bond lengths of rutile contained in pure titania and in the prepared samples fired at the different temperatures and distortion of TiO_6 octahedron (BLD). Values calculated from the Rietveld refinements of X-ray diffraction patterns.

Sample	Ti–O bond length (Å)			Distortion of TiO_6 octahedron (BLD)
	Apical distance (2×)	Basal distance (4×)	Average distance (6×)	
P25	2.068(18)	1.893(11)	1.951(13)	2.392
P25 900	1.981(2)	1.948(1)	1.959(1)	0.441
Si0.1 900	1.983(2)	1.947(1)	1.959(1)	0.485
Si0.3 900	1.984(3)	1.947(2)	1.959(2)	0.501
Si0.5 900	1.989(4)	1.943(3)	1.958(3)	0.625
P25 1000	1.981(2)	1.948(1)	1.959(1)	0.445
Si0.1 1000	1.987(3)	1.944(1)	1.959(2)	0.579
Si0.3 1000	1.978(4)	1.950(2)	1.959(3)	0.380
Si0.5 1000	1.989(4)	1.943(3)	1.958(3)	0.632
P25 1200	1.982(3)	1.947(2)	1.959(2)	0.481
Si0.1 1200	1.987(2)	1.944(2)	1.959(2)	0.585
Si0.3 1200	1.983(3)	1.948(2)	1.960(2)	0.475
Si0.5 1200	1.988(2)	1.946(1)	1.960(1)	0.577

Note: values in parentheses are the standard deviations referred to the last decimal figure.

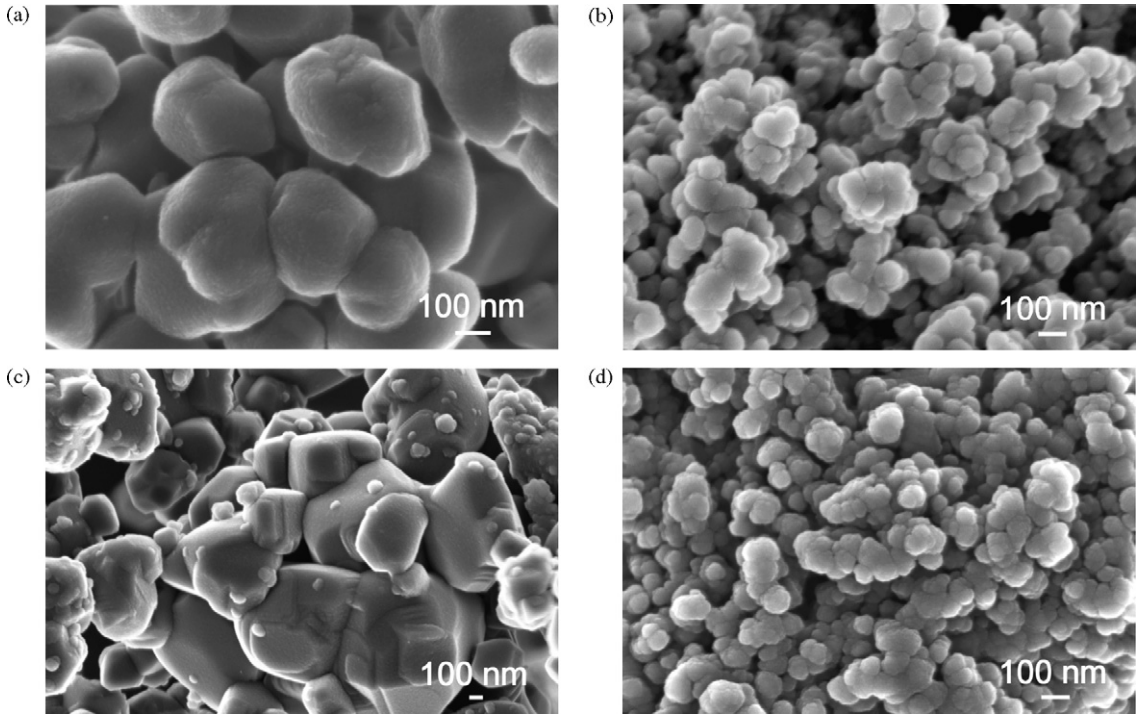

Fig. 2. FE-SEM micrographs: (a) sample P25 fired at 900 °C; (b) sample Si0.1 fired at 900 °C; (c) sample P25 fired at 1000 °C; (d) sample Si0.1 fired at 1000.

assigned to the asymmetric stretching vibration of Si–O–Si bond in the amorphous silica[47] surrounding the titania particles, as evidenced by TEM observations (Fig. 3).

The optical spectra of the samples illustrate how the addition of silica and the subsequent firing do not modify titania band gap (Fig. 6), since silica was not incorporated into titania structure. As a matter of fact, the onset of the absorption spectra appears to be at about 380–410 nm, that corresponds to anatase and rutile band gap (3.2 and 3.0 eV, respectively).[48] Those powders are actually a mixture of anatase and rutile, a part from P25 samples fired at the several temperatures – composed of rutile – whose absorption spectra are slightly shifted toward lower energies.

XPS spectrum of sample Si0.1 fired at 900 °C shows that the amounts of Ti (11.7 at%) and Si (9.8 at%) on the outer shell of the particle are approximately the same (Table 6). The O 1s core level spectra of the samples P25 and Si0.1, fired at 900 °C, are shown in Fig. 7. P25 spectrum can be decomposed into two contributions: a major peak at 529.8 eV with a small shoulder

Table 5
Mean anatase and rutile crystallite dimension and BET surface area of the prepared samples.

Sample	Anatase (nm)	Rutile (nm)	S_{BET} ($m^2\ g^{-1}$)
P25	23	35	50.0
P25 900	–	103	3.6
Si0.1 900	35	65	32.7
Si0.3 900	27	51	83.0
Si0.5 900	26	41	125.9
P25 1000	–	113	1.8
Si0.1 1000	38	72	25.9
Si0.3 1000	29	59	70.9
Si0.5 1000	28	49	103.7
P25 1200	–	126	1.2
Si0.1 1200	–	99	0.6
Si0.3 1200	[a]	74	0.8
Si0.5 1200	[a]	66	0.5

[a] The anatase amount in the mixture resulted to be too low for a reliable measure.

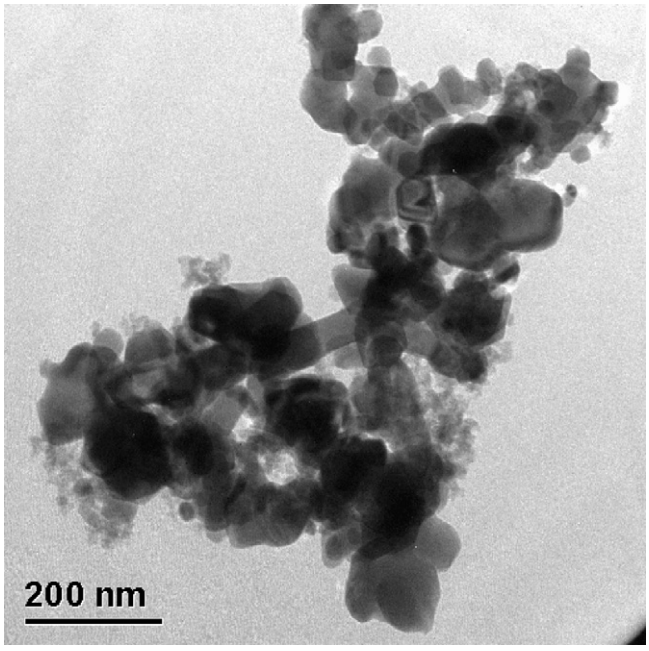

Fig. 3. TEM micrograph of the sample Si0.1 fired at 900 °C.

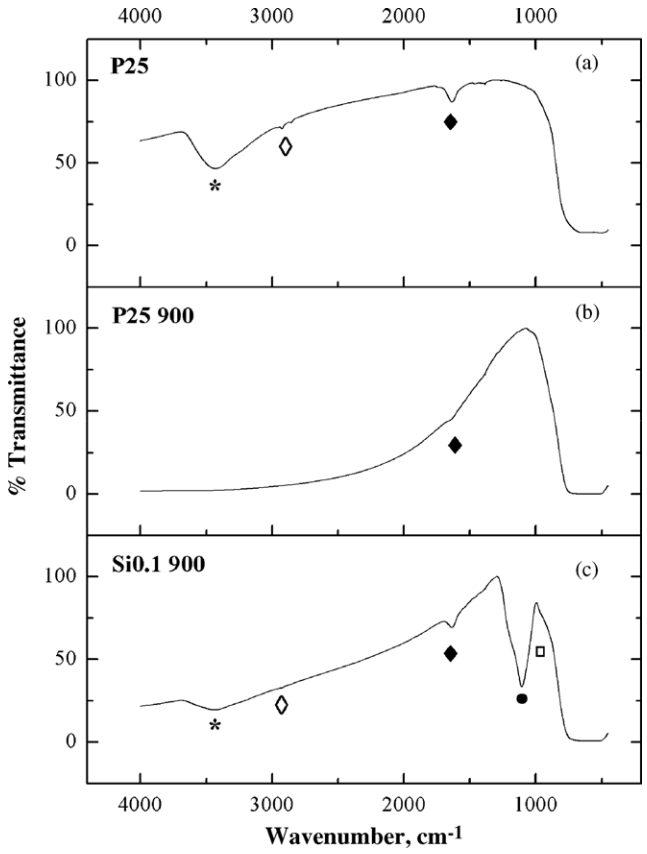

Fig. 4. FT-IR spectra of the samples: (a) P25 at room temperature; (b) P25 fired at 900 °C; (c) Si0.1 fired at 900 °C. *: hydroxyl groups; ♦: O–H bending vibrations; ◊: adsorbed water; □: Ti–O–Si bonds; ●: Si–O–Si bonds.

at 531.6 eV, respectively assigned to Ti–O in TiO_2, and to O–H adsorbed on the sample surface[49] according to FT-IR analysis. Besides these peaks, sample Si0.1 spectrum has another major peak at 532.9 eV, attributed to Si–O in SiO_2.[50]

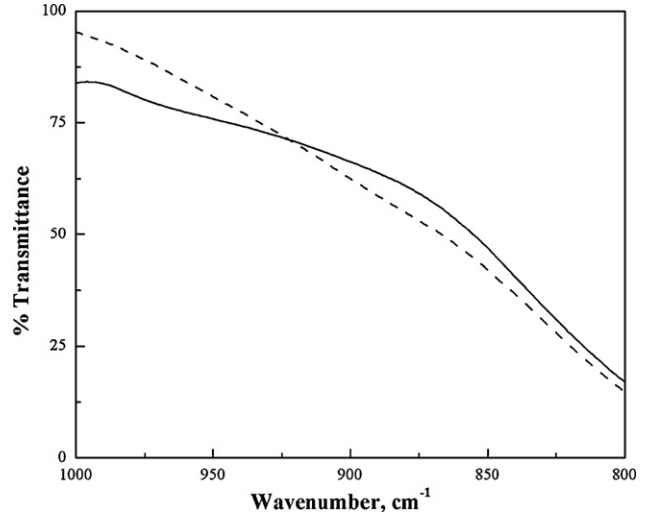

Fig. 5. Magnification in the range 1000–800 cm^{-1} of FT-IR spectra *b* and *c* reported, in order to emphasize the band at approximately 960 cm^{-1}, due to Ti–O–Si bonds. Dashed line: sample P25 fired at 900 °C; continuous line: sample Si0.1 fired at 900 °C.

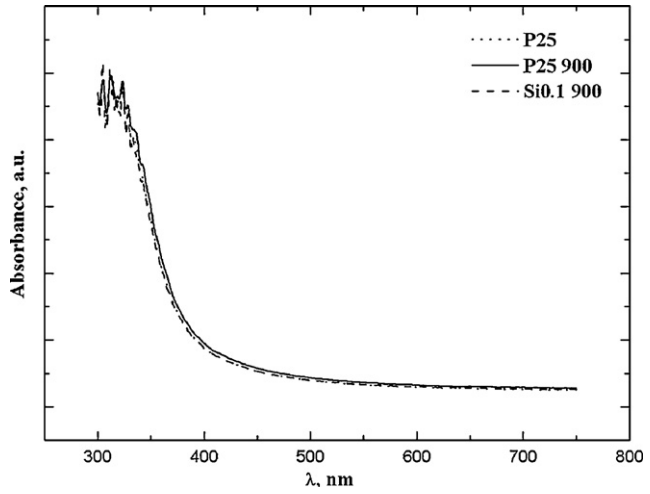

Fig. 6. DRS spectra of samples P25 at room temperature (dotted line) and samples P25 (continuous line) and Si0.1 (dashed line), both fired at 900 °C.

Table 6
Composition (at%) of samples P25 and Si0.1 fired at 900 °C, according to XPS analysis. Carbon comes from atmospheric CO_2.

Sample	Atomic %			
	O	Ti	Si	C
P25 900	60.1	19.4	–	20.5
Si0.1 900	59.1	11.7	9.8	19.4

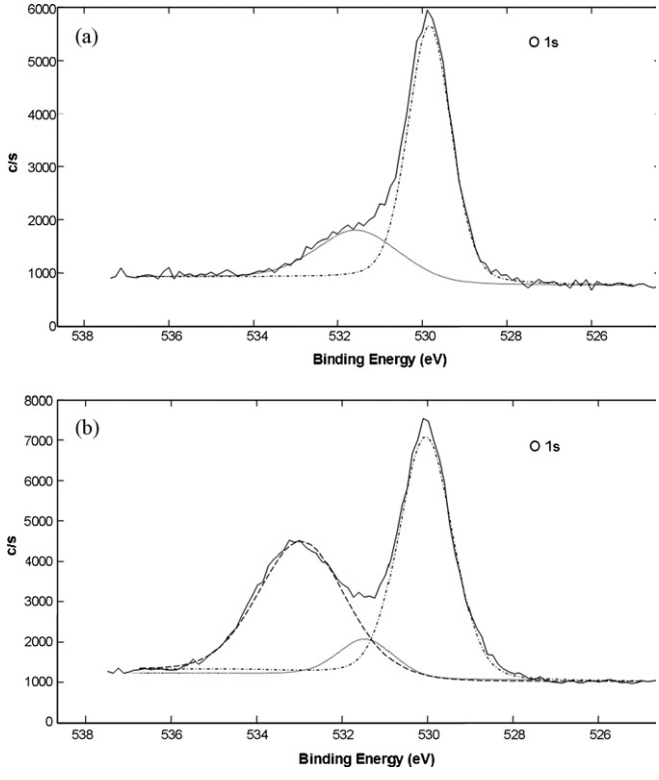

Fig. 7. XPS O1s core level spectra of the samples: (a) P25 fired at 900 °C; (b) Si0.1 fired at 900 °C. Dot-dash line: Ti–O bond; dotted line: O–H bond; dashed line: Si–O bond.

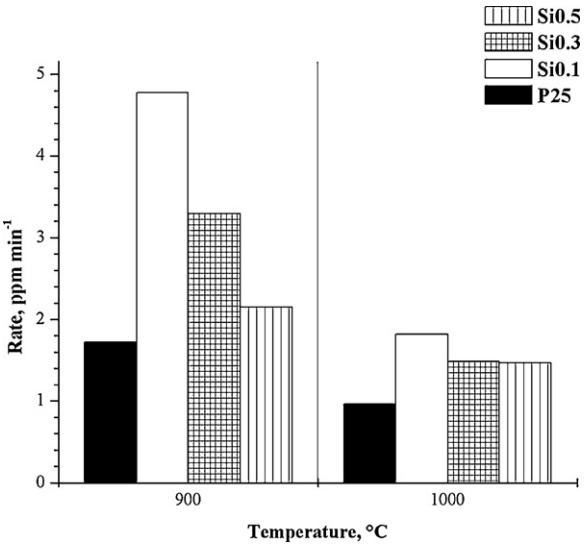

Fig. 8. Photocatalytic activity of the samples fired at 900 and 1000 °C, considered as the initial acetone formation rate.

3.3. Photocatalytic activity

The photocatalytic activity results are illustrated in Fig. 8. The presence of silica clearly improved the photocatalytic activity of titania samples, both at 900 and 1000 °C. No sample, which was thermally treated at 1200 °C, acted as a photocatalyst because of sintering that made particles bigger and gave the lowest surface area values.

Concerning the samples thermally treated at 900 °C, it is worth noting that rutile plays a significant role in the photocatalytic degradation.[51] Actually, sample P25 900, notwithstanding the lack of anatase, has a low but still appreciable photocatalytic activity, which is due to its crystallite size rather small, 103 nm. At 900 °C, the photocatalytic activity of the samples with silica addition improved, despite the presence of a not negligible amount of rutile and amorphous phase as well, as detected by XRPD (Table 2). Sample Si0.1 shows the best photocatalytic performances due to the less amount of amorphous phase (8.0 wt%), small anatase and rutile crystallite size and a high surface area value. Apart from that sample, more silica addition lowers the photocatalytic activity. This behaviour could be ascribed to the larger amount of amorphous phase that, surrounding titania particles, hinders its photocatalytic activity. In fact, the worst photocatalyst among the samples in which silica was added, is sample Si0.5 900 – the one containing the largest amount of amorphous phase at 900 °C. It can be asserted that the improved photocatalytic activity of Si0.1 900, compared to the reference sample (P25 900), is due to the presence of both anatase and rutile, characterised by small particle size and, consequently, to the high surface area value that increases the number of active sites participating in the photoreaction. The increase of the thermal treatment temperature, 1000 °C, causes a general decrease of the photocatalytic activity. This is more evident in the reference sample and in the samples where silica addition was more than 0.1 apfu. The biggest crystallite size and lowest surface area are responsible, for sample P25, of this behaviour. Samples Si0.3 and Si0.5, even if fired at 1000 °C, maintain a rather low crystallite size, in the range of 28–29 nm for anatase and 49–59 nm for rutile, consequently, surface area values are still high (Table 4). Nevertheless, they contain a large amount of amorphous phase that is strongly detrimental to their photocatalytic activity. It is highly probable that this detrimental effect is even higher in the case of increased rutile amount. Conversely, sample Si0.1 – having less amorphous SiO_2 amount, namely 8.0 wt% – is the best photocatalyst among the samples fired at that temperature, despite the presence of 88.1 wt% of rutile and the biggest anatase and rutile mean crystallite size within the set of Si-samples fired at 1000 °C (Tables 2 and 4).

Furthermore, the presence of more surface hydroxyl groups owing to silica addition, as detected by FT-IR analysis, favours the photocatalytic reaction, because it helps generating chemical oxidative species such as hydroxyl radicals that open the photocatalytic oxidation.[52] In addition, as revealed by the microscopic and XPS observations, amorphous SiO_2, present as a matrix between titania particles, acts as adsorbent domain, whereas TiO_2 as photocatalyst[22] (Figs. 3 and 6).

4. Conclusions

Silica was added to a titania powder in order to shift the anatase-to-rutile phase transition toward higher temperatures so as to improve its photocatalytic activity, once fired at high temperature.

The crystal structure of the fired powders was investigated thoroughly. Results validated as essentially no solid solution between the two crystalline end-members occurs; anyway, silica addition shifted toward higher temperatures the A → R polymorphic transformation by delaying anatase from reaching the critical size beyond which the phase transformation takes place, allowing therefore higher anatase retention.

An excessive amount of the amorphous phase, that surrounds the anatase/rutile particles, is able to decrease the photocatalytic performance of the sample. The ones containing less amorphous phase, behaved as the more active photocatalysts, both at 900 and 1000 °C. At the maximum firing temperature, 1200 °C, no sample acted as a photocatalyst, because of a partial sintering. The rutile contribution on the photocatalytic activity resulted to be not negligible.

The improved photocatalytic effects of silica addition in titania powders are supposed to be due to the smaller mean crystallite size and larger surface area, to the concurrent presence of anatase and rutile and to the more surface hydroxyl groups adsorbed on the photocatalyst surface.

Acknowledgements

The authors gratefully acknowledge Dr S.D. Škapin, Dr J. Kovač (Jožef Stefan Institute, Ljubljana) and Dr A. Sola (University of Modena and Reggio Emilia) for their helpful discussions. We are indebted to Prof A.G. Gualtieri (University of Modena and Reggio Emilia) for providing XRPD data. Constructive comments by an anonymous reviewer improved noticeably the final version of the manuscript.

References

1. Banfield JF, Veblen DR. Conversion of perovskite to anatase and TiO_2 (B): a TEM study and the use of fundamental building blocks for understanding relationships among the TiO_2 minerals. *Am Miner* 1992;**77**: 545–57.
2. Li J-G, Ishigaki T. Brookite → rutile phase transformation of TiO_2 studied with monodispersed particles. *Acta Mater* 2004;**52**:5143–50.
3. Ovenstone J, Yanagisawa K. Effect of hydrothermal treatment of amorphous titania on the phase change from anatase to rutile during calcinations. *Chem Mater* 1999;**11**:2770–4.
4. Fujishima A, Zhang X, Tryck DA. TiO_2 photocatalysis and related surface phenomena. *Surf Sci Rep* 2008;**63**:515–82.
5. Fox MA, Dulay MT. Heterogeneous photocatalysis. *Chem Rev* 1993;**93**:341–57.
6. Fujishima A, Rao TN, Tryk DA. Titanium dioxide photocatalysis. *J Photochem Photobiol C* 2000;**1**:1–21.
7. Fujishima A, Zhang X. Titanium dioxide photocatalysis: present situation and future approaches. *C R Chim* 2006;**9**:750–60.
8. Bosc F, Ayral A, Keller N, Keller V. Room temperature visible light oxidation of CO by high surface area rutile TiO_2-supported metal photocatalyst. *Appl Catal B: Environ* 2007;**69**:133–7.
9. Hidalgo MC, Maicu M, Navío JA, Colón G. Photocatalytic properties of surface modified platinised TiO_2: effects of particle size and structural composition. *Catal Today* 2007;**129**:43–9.
10. Burdett JK, Hughbanks T, Miller GJ, Richardson Jr JW, Smith V. Structural-electronic relationships in inorganic solids: powder neutron diffraction studies of the rutile and anatase polymorphs of titanium dioxide at 15 and 295 K. *J Am Chem Soc* 1997;**109**:3639–46.
11. Swope RJ, Smyth JR, Larson AC. H in rutile-type compounds: I. Single-crystal neutron and X-ray diffraction study of H in rutile. *Am Miner* 1995;**80**:448–53.
12. Shannon RD, Pask JA. Kinetics of the anatase–rutile transformation. *J Am Ceram Soc* 1965;**48**(8):391–8.
13. Kumar K-NP. Growth of rutile crystallites during the initial stage of anatase-to-rutile transformation in pure titania and in titania–alumina composites. *Scr Metall Mater* 1995;**32**:873–7.
14. Shannon RD, Pask JA. Topotaxy in the anatase–rutile transformation. *Am Miner* 1964;**49**:1707–17.
15. Ding X-Z, Liu X-H, He Y-Z. Grain size dependence of anatase-to-rutile structural transformation in gel-derived nanocrystalline titania powders. *J Mater Sci Lett* 1996;**15**(20):1789–91.
16. Gribb AA, Banfield JF. Particle size effects on transformation kinetics and phase stability in nanocrystalline TiO_2. *Am Miner* 1997;**82**:717–28.
17. Gamboa JA, Pasquevich DM. Effect of chlorine atmosphere on the anatase–rutile transformation. *J Am Ceram Soc* 1992;**75**(11):2934–8.
18. Matteucci F, Cruciani G, Dondi M, Raimondo M. The role of counterions (Mo, Nb, Sb, W) in Cr-, Mn-, Ni- and V-doped rutile ceramic pigments. Part 1. Crystal structure and phase transformation. *Ceram Int* 2006;**32**:385–92.
19. Linsebigler AL, Lu G, Yates JT. Photocatalysis on TiO_2 surfaces: principles, mechanisms, and selected results. *Chem Rev* 1995;**95**:735–58.
20. Hoffmann MR, Martin ST, Choi W, Bahnemann DW. Environmental applications of semiconductor photocatalysis. *Chem Rev* 1995;**95**:69–96.
21. Agrios AG, Pichat P. Recombination rate of photogenerated charges versus surface area: opposing effects of TiO_2 sintering temperature on photocatalytic removal of phenol, anisole, and pyridine in water. *J Photochem Photobiol A: Chem* 2006;**180**:130–5.
22. Anderson C, Bard AJ. Improved photocatalytic activity and characterization of mixed TiO_2/SiO_2 and TiO_2/Al_2O_3 materials. *J Phys Chem B* 1997;**101**:2611–6.
23. Fu X, Clark LA, Yang Q, Anderson MA. Enhanced photocatalytic performance of titania-based binary metal oxides: TiO_2/SiO_2 and TiO_2/ZrO_2. *Environ Sci Technol* 1996;**30**:647–53.
24. Anderson C, Bard AJ. An improved photocatalyst of TiO_2/SiO_2 prepared by a sol–gel synthesis. *J Phys Chem* 1995;**99**:9882–5.
25. Xie C, Xu Z, Yang Q, Xue B, Du Y, Zhang J. Enhanced photocatalytic activity of titania-silica mixed oxide prepared via basic hydrolyzation. *Mater Sci Eng B* 2004;**112**:34–41.
26. Circone S, Agee CB. Effect of pressure on cation partitioning between immiscible liquids in the system TiO_2–SiO_2. *Geochim Cosmochim Acta* 1995;**59**:895–907.
27. DeVries RC, Rustum R, Osborn EF. The system TiO_2–SiO_2. *Trans Br Ceram Soc* 1954;**53**:525–40.
28. Tobaldi DM, Tucci A, Camera-Roda G, Baldi G, Esposito L. Photocatalytic activity for exposed building materials. *J Eur Ceram Soc* 2008;**28**:2645–52.
29. Gualtieri AF, Brignoli G. Rapid and accurate quantitative phase analysis using a fast detector. *J Appl Crystallogr* 2004;**37**:8–13.
30. Larson AC, Von Dreele RB. *General structure analysis system (GSAS)*. Los Alamos National Laboratory Report LAUR; 2000. pp. 86–784.
31. Toby BH. EXPGUI, a graphical user interface for GSAS. *J Appl Crystallogr* 2001;**34**:210–3.
32. Howard CJ, Sabine TM, Dickson F. Structural and thermal parameters for rutile and anatase. *Acta Crystallogr* 1991;**B47**:462–8.
33. Gualtieri AF. Accuracy of XRPD QPA using the combined Rietveld—RIR method. *J Appl Crystallogr* 2000;**33**:267–78.
34. Renner B, Lehmann G. Correlation of angular and bond length distortions in TO_4 units in crystals. *Zeit Krist* 1986;**175**:43–59.
35. Klug HP, Alexander EL. *X-ray diffraction procedures for polycrystalline and amorphous materials*. 2nd ed. New York, USA: J. Wiley and Sons; 1974. p. 960.
36. Senthilkumaar S, Porkodi K, Vidyalakshmi R. Photodegradation of a textile dye catalyzed by sol–gel derived nanocrystalline TiO_2 via ultrasonic irradiation. *J Photochem Photobiol A* 2005;**170**:225–32.
37. Ohko Y, Fujishima A, Hashimoto K. Kinetic analysis of the photocatalytic degradation of gas-phase 2-propanol under mass transport-limited conditions with a TiO_2 film photocatalyst. *J Phys Chem B* 1998;**102**:1724–9.
38. Yoshinaka M, Irota K, Yamaguchi O. Formation and sintering of TiO_2 (anatase) solid solution in the system TiO_2–SiO_2. *J Am Ceram Soc* 1997;**80**(10):2749–53.
39. Shannon RD. Revised effective ionic radii and systematic studies of interatomic distances in halides and chalcogenides. *Acta Crystallogr* 1976;**A32**:751–67.
40. Viswanath RN, Ramasamy S. Study of TiO_2 nanocrystallites in TiO_2–SiO_2 composites. *Colloid Surf A* 1998;**133**:49–56.
41. Jamnik J, Dominko R, Erjavec B, Remškar M, Pintar A, Gaberščček M. Stabilizers of particle size and morphology: a road towards high-rate performance insertion materials. *Adv Mater* 2009;**21**:2715–9.
42. Reidy DJ, Holmes JD, Morris MA. The critical size mechanism for the anatase to rutile transformation in TiO_2 and doped-TiO_2. *J Eur Ceram Soc* 2006;**26**:1527–34.
43. Hou YD, Wang XC, Wu L, Chen XF, Ding ZX, Wang XX, et al. N-doped SiO_2/TiO_2 mesoporous nanoparticles with enhanced photocatalytic activity under visible-light irradiation. *Chemosphere* 2008;**72**:414–21.
44. He C, Tian B, Zhang J. Synthesis of thermally stable and highly ordered bicontinuous cubic mesoporous titania–silica binary oxides with crystalline framework. *Micropor Mesopor Mater* 2009;**126**:50–7.
45. Ukmar T, Godec A, Maver U, Planinšek O, Bele M, Jamnik J, et al. Suspensions of modified TiO_2 nanoparticles with supreme UV filtering ability. *J Mater Chem* 2009;**19**:8176–83.
46. Guan K, Lu B, Yin Y. Enhanced effect and mechanism of SiO_2 addition in super-hydrophilic property of TiO_2 films. *Surf Coat Technol* 2003;**173**:219–23.
47. Gärtner M, Dremov V, Müller P, Kish H. Bandgap widening of titania though semiconductor support interactions. *Chem Phys Chem* 2005;**6**:714–8.
48. Fujishima A, Zhang X, Tryk DA. TiO_2 photocatalysis and related surface phenomena. *Surf Sci Rep* 2008;**63**:515–82.
49. Liu H, Yang W, Ma Y, Cao Y, Yao J, Zhang J, et al. Synthesis and characterization of titania prepared by using a photoassisted sol–gel method. *Langmuir* 2003;**19**:3001–5.
50. Yu J-G, Yu H-G, Cheng B, Zhao X-J, Yu JC, Ho W-K. The effect of calcination temperature on the surface microstructure and photocatalytic activity

of TiO_2 thin films prepared by liquid phase deposition. *J Phys Chem B* 2003;**107**:13871–9.

51. Ding Z, Lu GQ, Greenfield PF. Role of the crystallite phase of TiO_2 in heterogeneous photocatalysis for phenol oxidation in water. *J Phys Chem B* 2000;**104**:4815–20.
52. Balasubramanian G, Dionysiou DD, Suidan MT, Bauidin I, Laîne J-M. Evaluating the activities of immobilized TiO_2 powder films for the photocatalytic degradation of organic contaminants in water. *Appl Catal B: Environ* 2004;**47**:73–84.